A BIDIRECTIONAL BATTERY CHARGER FOR A BROAD RANGE OF ELECTRIC VEHICLES

Mr. P. Uday Kumar[1], B. Sai pavan Kumar[2], T. Venkata Krishna[3], SK. Karimulla[4] [1]Assistant Professor,
Department of EEE, Sree vahini institute of science and Technology., Tiruvuru., NTR District., AP, India
[2,3,4]UG scholar students Sree vahini institute of science and technology.,Tiruvuru.,NTR District., AP, India

ABSTRACT:-

This paper describes the design and functioning of a modified SEPIC converter-based bidirectional battery charger for a variety of electric vehicles (EVs). The diverse variety of EVs comprises an electric two-wheeler (e2W) and an electric automobile. As a result, a modified SEPIC converter is designed to charge both an e2W with a 72 V battery and an electric automobile with a 240 V battery. The presented battery charger has the significant advantage of complying with the IEC standard in addition to providing good charging performance. Furthermore, the redesigned SEPIC converter-based battery charger offers bidirectional operation. The efficiency of the given battery charger grid to a vehicle (G2V) is tested using the optimal grid voltage. Furthermore, the charger's efficacy is tested using amplitude fluctuations in grid voltage. Finally, the given charger is evaluated for a vehicle-to-home (V2H) operation to demonstrate the efficacy of the bidirectional operation.

Index Terms: Battery Charger, DC/DC Converter, AC/DC Converter, and Power Quality.

I.INTRODUCTION

Battery charger technology has recently evolved into two categories: unidirectional chargers and bidirectional chargers. Modern unidirectional battery chargers [1-3] are designed to increase power density. In this context, the authors of [1] presented the bridgeless topology of the battery charger for low voltage battery-powered electric vehicles (EV). The advantages of this charger are its high efficiency and power density. Keeping high efficiency in mind, the authors of [2] proposed a resonant converter-based single-stage EV charger for high voltage battery-powered EVs. The given EV charger has low losses, which means it is highly efficient. Another scheme for a very high voltage driven battery is described in [3]. However, the aforementioned EV charging topologies are unidirectional.

The Modern bidirectional battery chargers [4]-[5] significantly improve the usability of EVs with vehicle-to-grid/home (V2G or V2H) operation. In light of this, the authors of [4] propose a bidirectional EV charger topology. The present charger supports four-quadrant operation and meets the necessary power quality standards [5]. In [6, the authors offer an electrolytic capacitor-less EV charger design with sinusoidal ripple charging. Furthermore, the authors examined the advantages of sinusoidal ripple current charging. However, the bidirectional topologies described above are two-stage topologies. As a result, the losses are substantially higher than in single-stage topologies.Aside from efficiency, the charger

topologies outlined above are only suited for a specific range of output voltage. Therefore, the EV charger with a wide output voltage range is to be explored. Keeping this in view, state-of-the-art EV chargers with wide output voltage ranges are discussed in [7]- [8]. In [7], a Vienna converter-based EV charger is presented. The authors have

mentioned that the key advantage of the provided topology is wide output voltage range capabilities. However, it is a unidirectional EV charger. The authors of [8] presented a topology capable of producing a wide range of output voltages while operating bidirectionally. However, the given EV charger topology is a two-stage EV charger.

Considering the constraints of the above-mentioned existing EV charge topologies, this work provides a single-stage bidirectional battery charger with a large output voltage range. In addition, the provided battery charger provides galvanic isolation to the battery of the car from the AC supply. The significant development of this study is as follows.

- The design and functioning of a modified SEPIC converter-based bidirectional battery charger with a broad output voltage range are described.
- The operation and control of the proposed charger architecture are discussed.
- A 1.1 kW system is built to test the effectiveness of the proposed charger during grid-to-vehicle (G2V) operation.
- The performance of the provided charger is confirmed using a 72 V battery and a 240 V battery at the output.
- The charging procedure of a 72 V battery corresponds to the charging of electric two-wheelers (e2W) at home. Furthermore, the charging operation 240 V battery indicates the charging of an electric automobile at home.
- The performance of the provided charger with different grid voltages is shown to demonstrate its usefulness.
- The V2H operation with a 240 V battery system is reviewed in order to demonstrate the effectiveness of the provided charger during bidirectional operation.

II. CONFIGURATION OF THE SYSTEM

Figure 1 depicts the presented EV charging setup. Clearly, the given charger is made up of two modified SEPIC bidirectional converter cells. In this, one cell of the SEPIC converter functions during the positive half-cycle. Another operates during the negative half-cycle of the grid voltage.

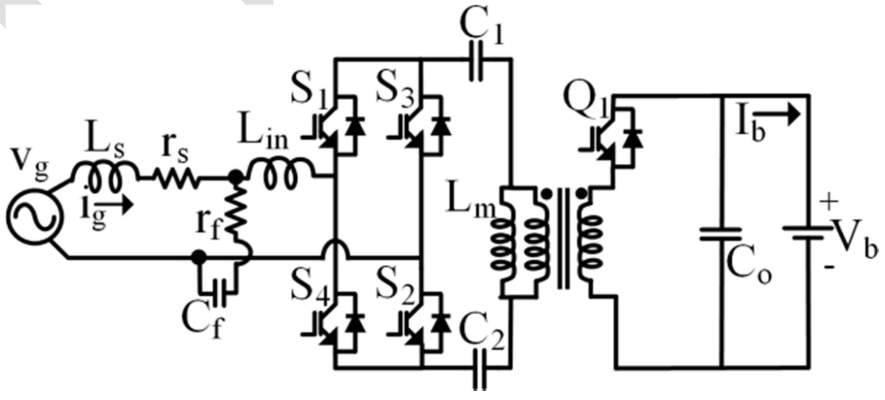

Fig. 1 Schematic circuit diagram of the presented charger.

In this approach, the current updated SEPIC converter-based AC/DC converter is a bidirectional bridgeless converter. This converter has an RC filter to reduce switching noise from the grid voltage. Furthermore, the input inductor, Lin, is meant to manage the grid current while transferring power from the AC supply to the EV battery. Notably, a high-frequency transformer is used with this charger. This transformer protects the battery from the AC supply by providing galvanic isolation. The transformer is designed in such a way that its magnetizing inductance acts in the discontinuous conduction mode (DCM). As a result, the DCM operation of this transformer achieves a unity power factor at the supply.

III.OPERATIONAL PRINCIPLE

The offered charger keeps the battery current constant during the G2V charging process. Furthermore, it adjusts the sinusoidal voltage at the load-charger junction during V2H operation. Figures 2-3 show circuit diagrams that explain the state of the components and the accompanying waveforms while keeping these operations in perspective. Figures 2(a)-(f) show that the proposed charger's operating modes during the positive half cycle are identical to those during the negative half cycle in both G2V and V2H operations. In this approach, the G2V operations during the positive half-cycle are described in full below.

Mode-I: To enter this mode, turn switches S3 and S4 "ON" during the positive half cycle of the grid voltage. Fig. 2(a) shows that the anti-parallel diode of switch S1 is forward biased, thus the inductor Lin charges through this diode and switches S3. Additionally, the capacitors C1 and C2 discharge via switches S3 and S4. Capacitors C1 and C2 store energy, which is transferred to the transformer's magnetizing inductor. As seen in Figure 2(a), the magnetizing inductance, Lm, begins to charge. The stored energy in the output capacitor is transferred to the battery, as shown in Fig. 2(a). Notably, Figure 3(a) shows the related inductor current and capacitor voltage waveforms, as well as the switching pulses.

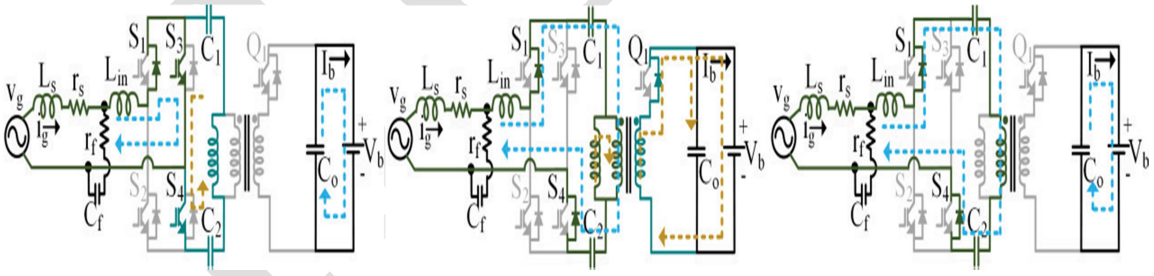

Fig. 2 EV charger operating modes (a)-(c) during the Positive half-cycle of gridvoltage.

Mode-II: The transition from mode-I to mode-II occurred when switches S3 and S4 were switched off. In this mode, the high-frequency transformer's magnetizing inductance transfers energy to the battery via transformer action. Figure 2(b) shows that when switches S3 and S4 are turned off, the stored inductor energy in Lin is supplied to capacitors C1 and C2. As a result, the capacitors begin to charge in this state. Because the transformer operates in DCM, this mode ends when the magnetizing inductance is fully discharged. The waveforms for this operation are shown in Figure 3(a).

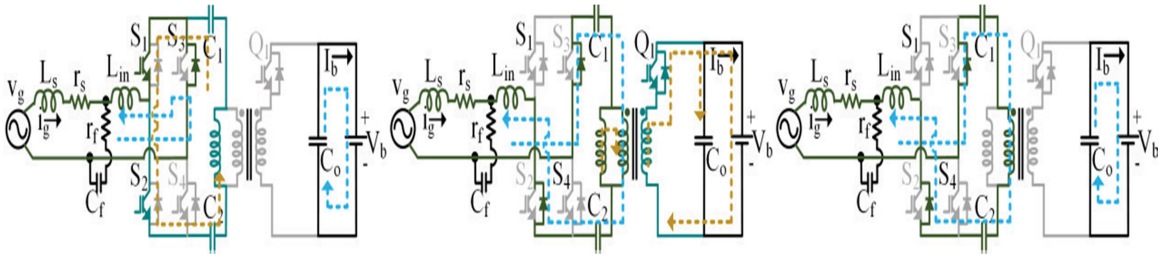

[D] [E] [F]

Fig. 2 EV charger operating modes (d)-(f) during the negative half-cycle of gridvoltage.

Mode-III: Because the magnetizing inductance has been completely drained, the transformer activity stops. As a result, during this working mode, capacitors C1 and C2 charge via the AC source, with no power transferred from the AC supply to the battery. In this mode, the battery charges by using the energy stored in the output capacitor. Figures 2 and 3 show the corresponding circuit diagram and relevant waveforms.

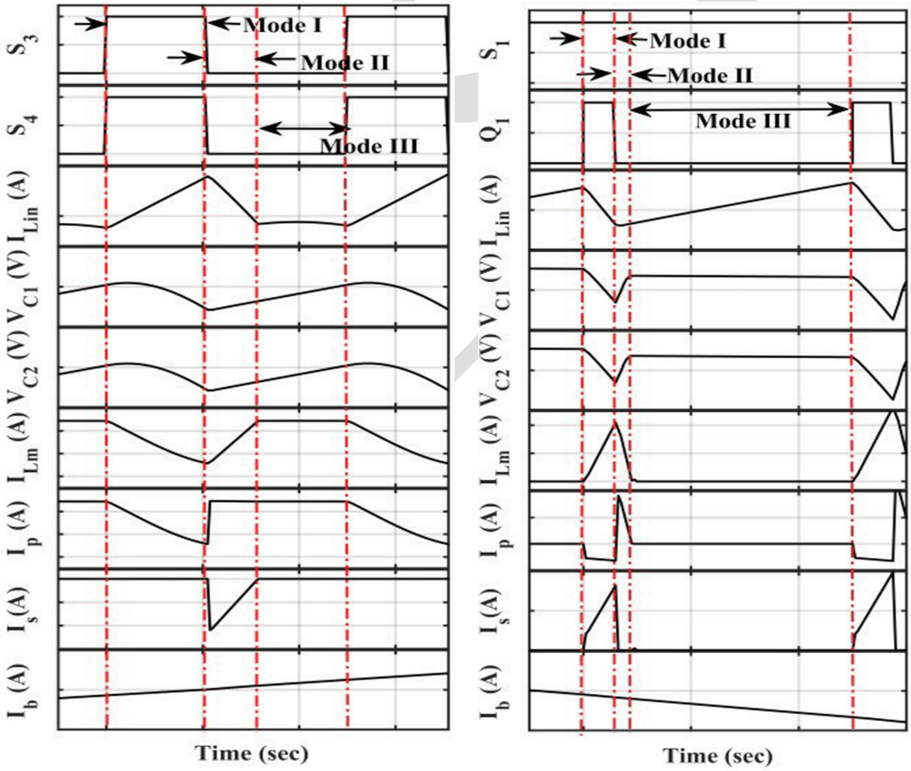

3[A] 3[B]

FIG 3[A]&[B] Shows the Wave Forms of Operating Conditions

The bidirectional operation of the provided charger is explained using the V2H operation. Figures 2(g)-(l) depict circuit diagrams of the operational modes during V2H operation. Notably, the operating modes throughout both half cycles of the grid voltage are identical; thus, the V2H operation during the positive half-cycle will be described in detail below.

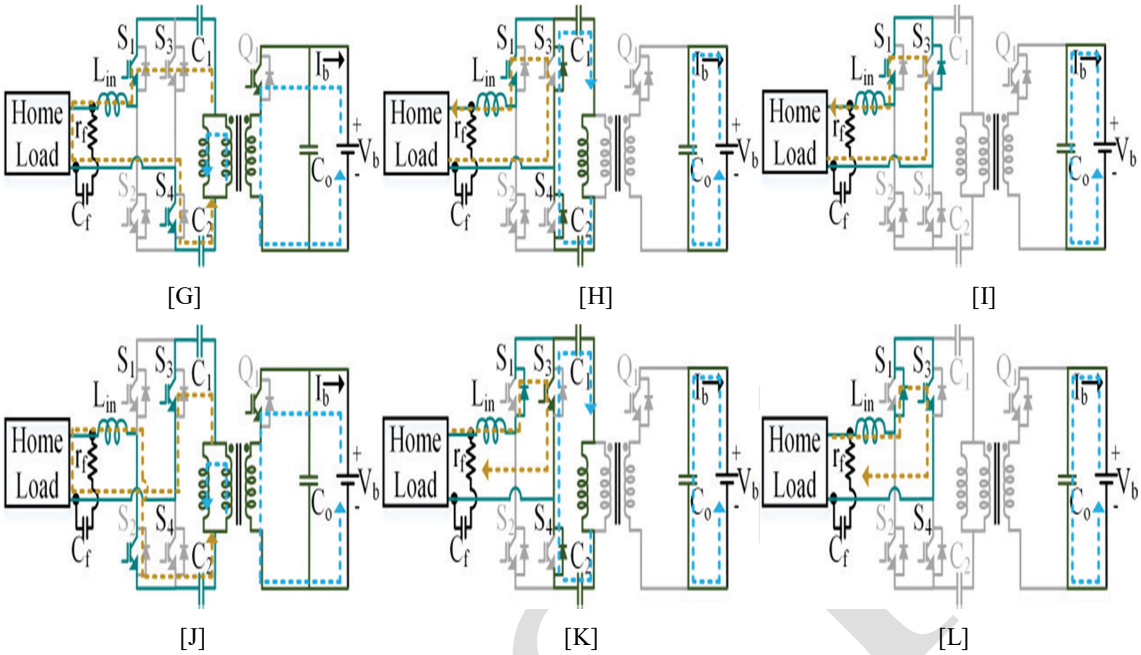

[G] [H] [I]

[J] [K] [L]

FIG 2(g)-(L) Shows The circuit diagrams of the operational modes during V2H operation.

Mode I: This mode begins when switch Q1 is turned "ON" while the V2H is operating in steady-state. This activates the transformer's magnetizing inductance. Furthermore, electricity is sent to residential loads using energy stored in the vehicle's capacitors C1 and C2, as well as its batteries. In this state, switches S1 and S4 are set to 'ON'. Figures 2(g) show the appropriate circuit diagrams that describe this operation, whereas Figure 3(b) shows the associated waveforms.

Mode II: Similar to the previous mode, this mode begins when switch Q1 is switched OFF. As shown in Fig. 2(h), the diodes of the switches S3 and S4 conduct in this mode, and capacitors charge using the stored energy in magnetizing inductance. Furthermore, the stored energy in the inductor Lin provides power to house loads, as seen in Fig. 2(h). The corresponding waveforms are shown in Fig. 3(b).

Mode III: begins when the magnetizing inductance stops charging the capacitor. During this operating mode, the stored energy in the inductor Lin powers the house loads, as shown in Fig 2(i). The waveforms for the operation are shown in Fig. 3(b).

IV.DESIGINING OF THE SYSTEM

The charger component is chosen based on the rated parameters and the aforementioned operating modes. The rating parameters are listed in Table I. Table-I also includes the estimated and selected values for the components' permissible voltage and current ripples. Notably, the charging operation at the rated condition is carried out using the maximum battery voltage at the output and the rated supply at the input. As a result, the duty ratio of the converter is computed taking into account the rated input voltage and the maximum output voltage. The other components of the charger are determined using this duty ratio.

Parameters	Design estimation	Remarks	Estimated value	Selected Value
L_{in}	$V_{g,\max} D_{\max} \quad f_s \Delta i_{Lin}$	D=0.28; f_s = 20 kHz; Δi_{Lin}=30% of i_{Lin}	2.32 mH	3 mH
$L_{m,C}$	$R_{Lmin} \quad f_s (1+2D \; D_C)$	f_s=20 kHz; RL=Vb/Ib ;	0.3 mH	60µH

TABLE I: Estimation of Parameters

V. CONTROL ALGORITHM

Figures 4(a)–(b) show the block diagrams of the controller for operations such as G2V and V2H. The controller's goal is to keep the battery current constant during this operation while also regulating power quality in accordance with appropriate requirements. In this concept, the converter's transformer is built to function in DCM. Furthermore, the transformer's DCM operation ensures that the grid current meets the necessary power quality standards. As a result, the controller's primary goal is to keep current flowing through the battery terminals while operating at G2V voltage. In addition, the controller of the proposed charger is responsible for maintaining the voltage at the point of common intersection of the load and the charger during V2H.The detailed discussion is as follows.

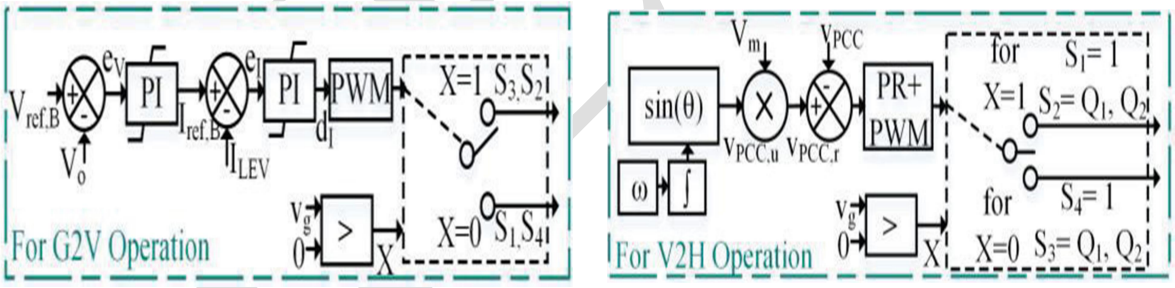

[A] **[B]**

FIG 4 shows a control block diagram.

A. Controller for G2V operation

The G2V functioning is controlled by a constant current charging algorithm. The control block diagram is shown in Figure 4(a). The battery current is measured and compared to the reference charging current, as shown in Figure 4(a). The proportional-integral (PI) regulator optimizes the error between the measured and reference battery currents.

This PI regulator uses the error to calculate the reference duty ratio, as shown in Fig. 4(a). These switching pulses are routed to switch pairs S1-S2 during the negative half cycle of the grid voltage and S3-S4 during the positive half cycle of the grid voltage. Notably, positive and negative half-cycle durations are estimated using the

comparator and measured grid voltage.

B.Controller for V2H Operation

As seen in Fig. 4(b), the control algorithm during the V2H operation is in charge of maintaining the sinusoidal voltage at the load's point of common intersecting (PCI) with the charger. To accomplish this, a reference voltage is created and compared to the observed voltage at the PCI. The estimated error is transmitted to the PR regulator. The PR regulator processes it and uses the estimated output for PWM switching. The controller governs switches Q1-S4 in pairs, and S1 and S2 based on the grid voltage's positive and negative half cycles, respectively. Notably, positive and negative half-cycle durations are estimated using the comparator and measured reference sinusoidal voltage.

VI. RESULTS AND DISCUSSIONS

The performance of the provided charger is as shown in below fig 5 is evaluated under ideal grid conditions and with grid voltage changes. In this context, the G2V operation with a 72 V and a 240 V battery validates the charger's ability to operate over a large output voltage range. The results are shown in Figures 6-8. Furthermore, the efficacy of the G2V operation with varied AC supply voltage amplitudes is investigated, and the results are given in Figs. 8(a)-(b). Furthermore, the provided charger's satisfactory behavior during V2H operation is validated, with findings shown in Figs. 9(a)-(b). The following is a full study of the cited results.

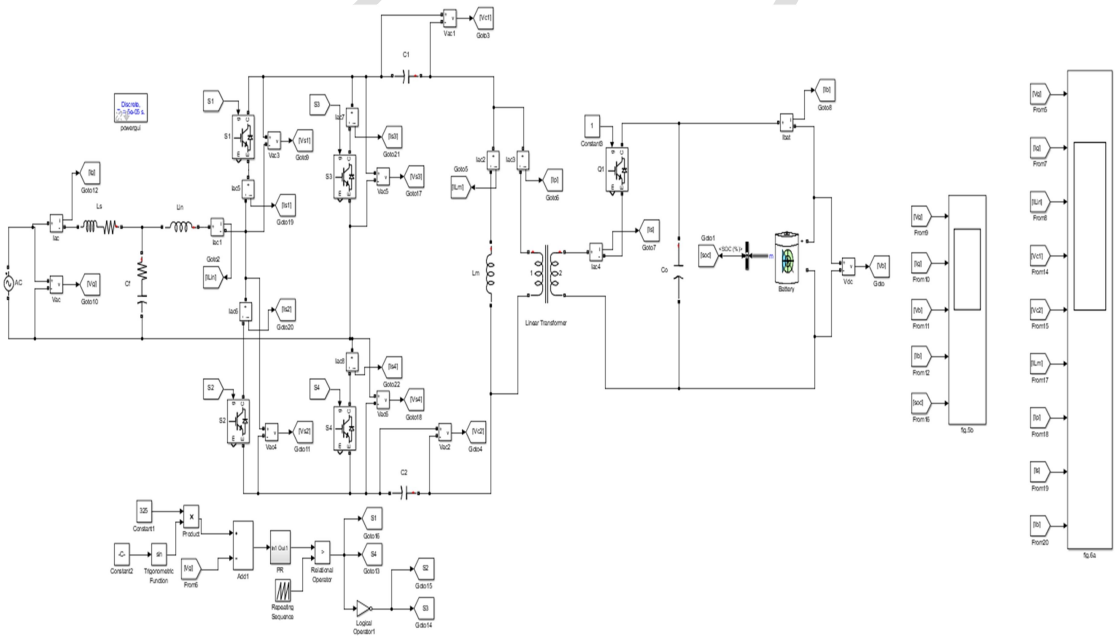

FIG 5 Simulink Diagram of Presented Charger

A.Charging operation with 72 V and 240 V battery

A 72 V and 240 V battery are charged to test the efficacy of the provided charger's wide output voltage range performance. The acquired findings are shown in Figure 6. Figure 6(a) shows that the grid voltage and current are in phase while charging a 72 V battery in a low voltage battery-powered car. Notably, the average battery current is set

at the reference current. Furthermore, the battery current ripples meet the necessary standards [9]. Furthermore, Fig. 6(a) shows that grid current THD is 3.46%, indicating compliance with applicable criteria for grid current quality. Figure 6(b) depicts the charging operation for the 240 V battery.

This shows the grid voltage and current in phase. Furthermore, the battery voltage is shown in Fig. 6(b). The average battery current when charging the 240 V battery is controlled, as shown in Fig. 6(b). Because the battery current ripples are within the acceptable limits, the controller design is adequate. Furthermore, the grid current THD is 1.11%, indicating that the operation meets applicable power quality standards. As a result, the given charger's design and control algorithm meet expectations.

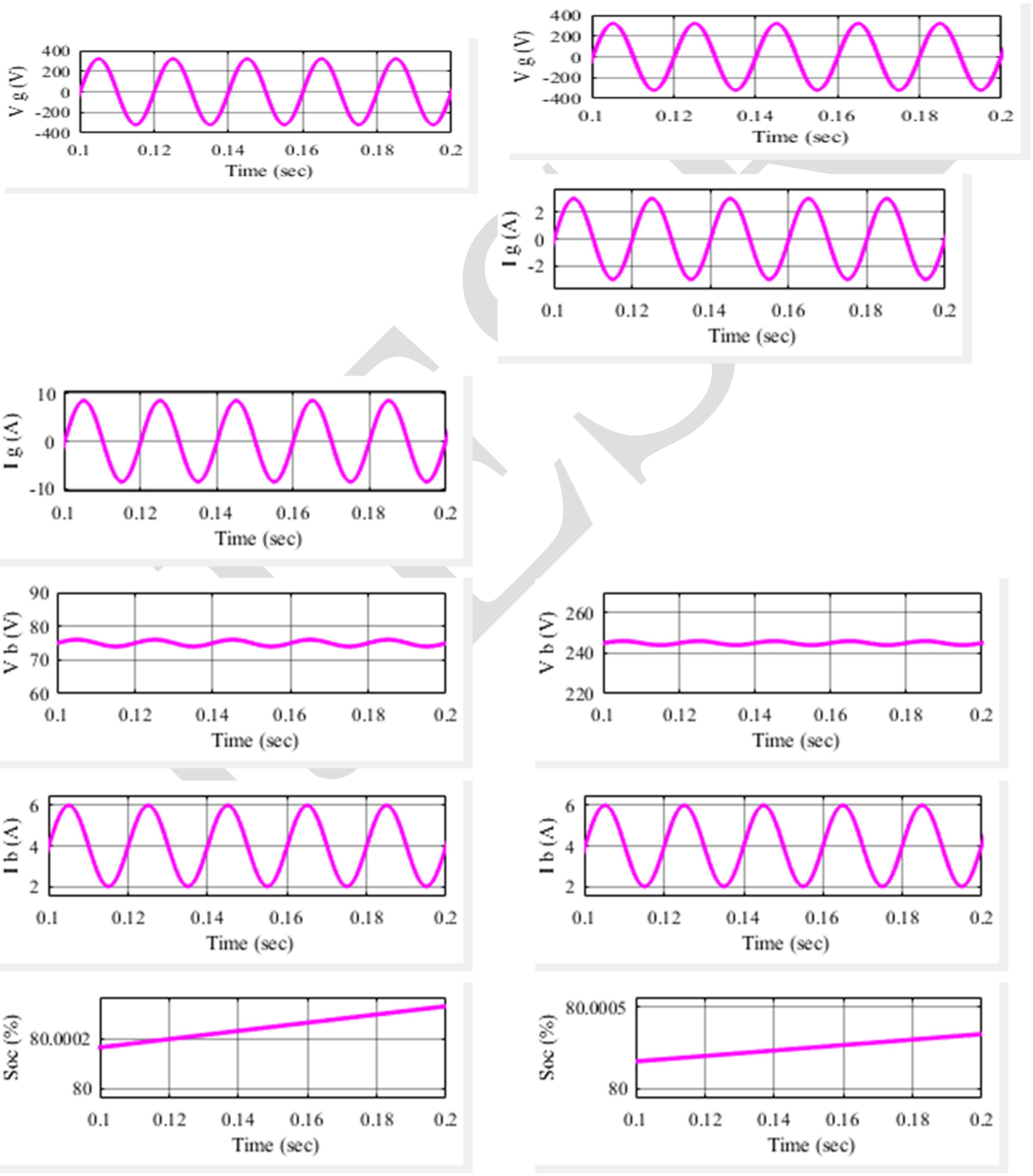

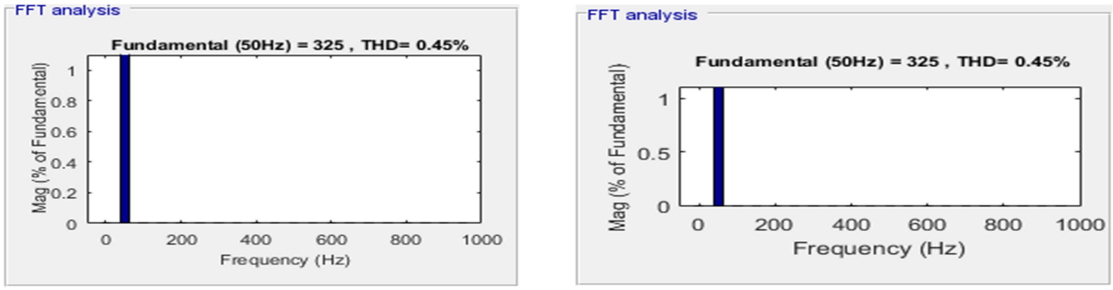

[A] [B]

Fig. 6 Results of regulated charging operation with (a) 72 V battery and (b) 240 V battery During G2V Operation

B. Performance Analysis of Charger during G2V Operation

Figure 7(a) shows the voltage and current strains over the charger components during G2V operation with a 72 V battery-powered vehicle. Figure 7(a) shows that the grid current follows the input inductor current iLin. Figure 7(a) shows that the capacitors C1 and C2 function in continuous conduction mode, while the voltages VC1 and VC2 are well regulated.

Furthermore, Figure 7(a) shows that the high-frequency transformer's magnetizing inductance functions in discontinuous conduction mode (DCM). Thus, the converter's design for 72 V battery charging is satisfactory.

Figure 7(b) depicts the voltage and current strains across the charger's passive components when a 240 V battery is being charged. The current stress via the input inductor, Lin, increases as power transfer increases during the charging of a high voltage charged battery. Notably, this process regulates the voltage across the capacitors C1 and C2. The ripples in the capacitor voltage are greater than when a 72 V battery is being charged. Furthermore, the DCM operation of the transformer's magnetizing inductance is validated, as seen in Fig. 7(b). The charger's design works well because the currents and voltages across the components are regulated.

Aside from the passive components, voltage and current stress, the voltage and current across the switches are analyzed, and the findings are presented in Figs. 8(a)–(b). Notably, the voltages/currents across/through the switches during G2V operation remain within the design limitations across the entire voltage range. Hence, the charger's design and control algorithm are satisfactory.

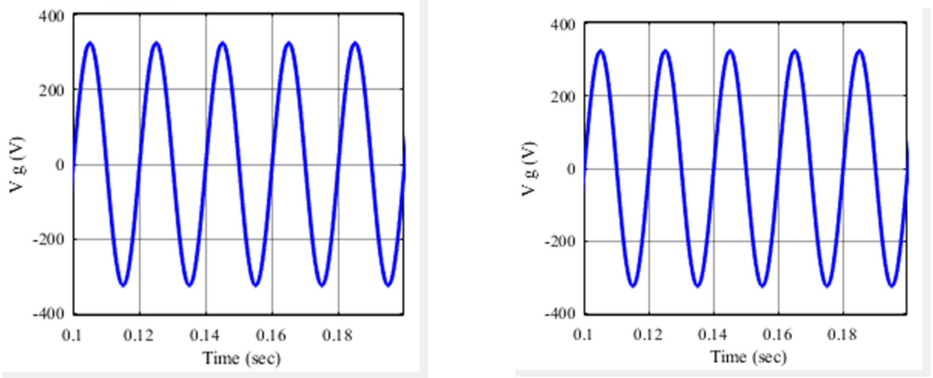

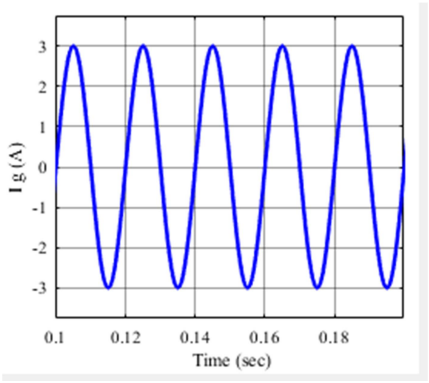
I g (A)
Time (sec)

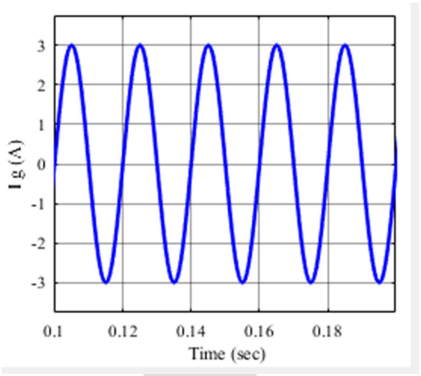
I g (A)
Time (sec)

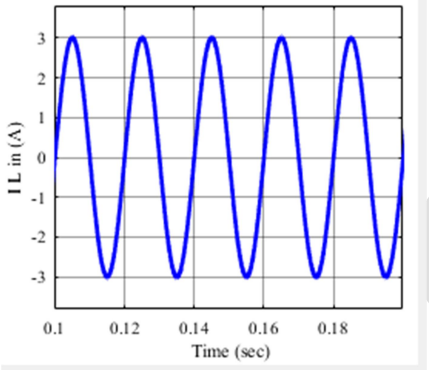
I L in (A)
Time (sec)

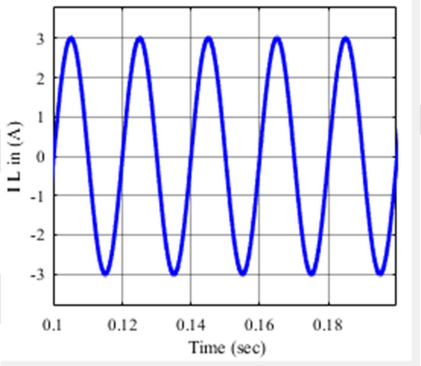
I L in (A)
Time (sec)

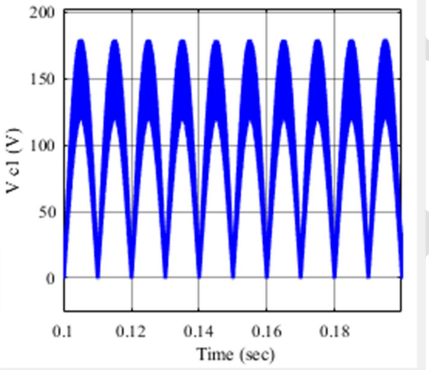
V c1 (V)
Time (sec)

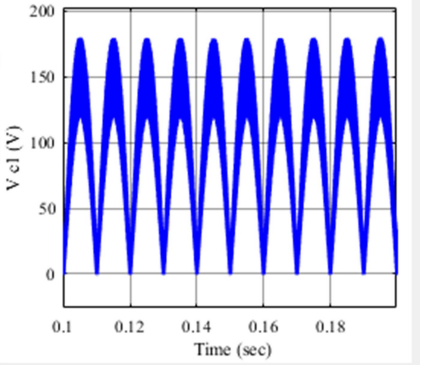
V c1 (V)
Time (sec)

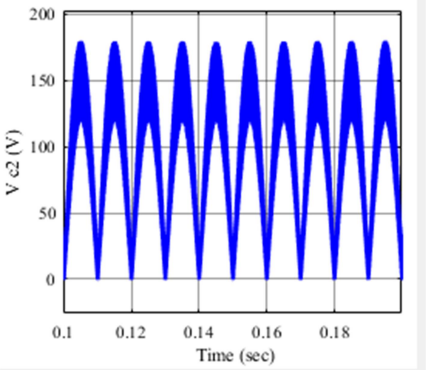
V c2 (V)
Time (sec)

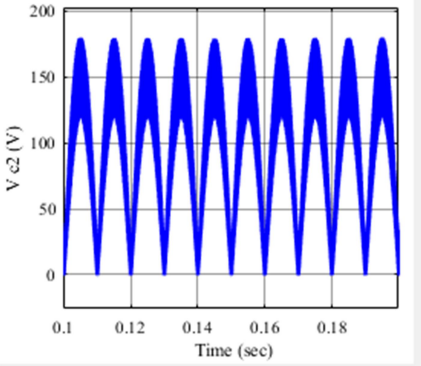
V c2 (V)
Time (sec)

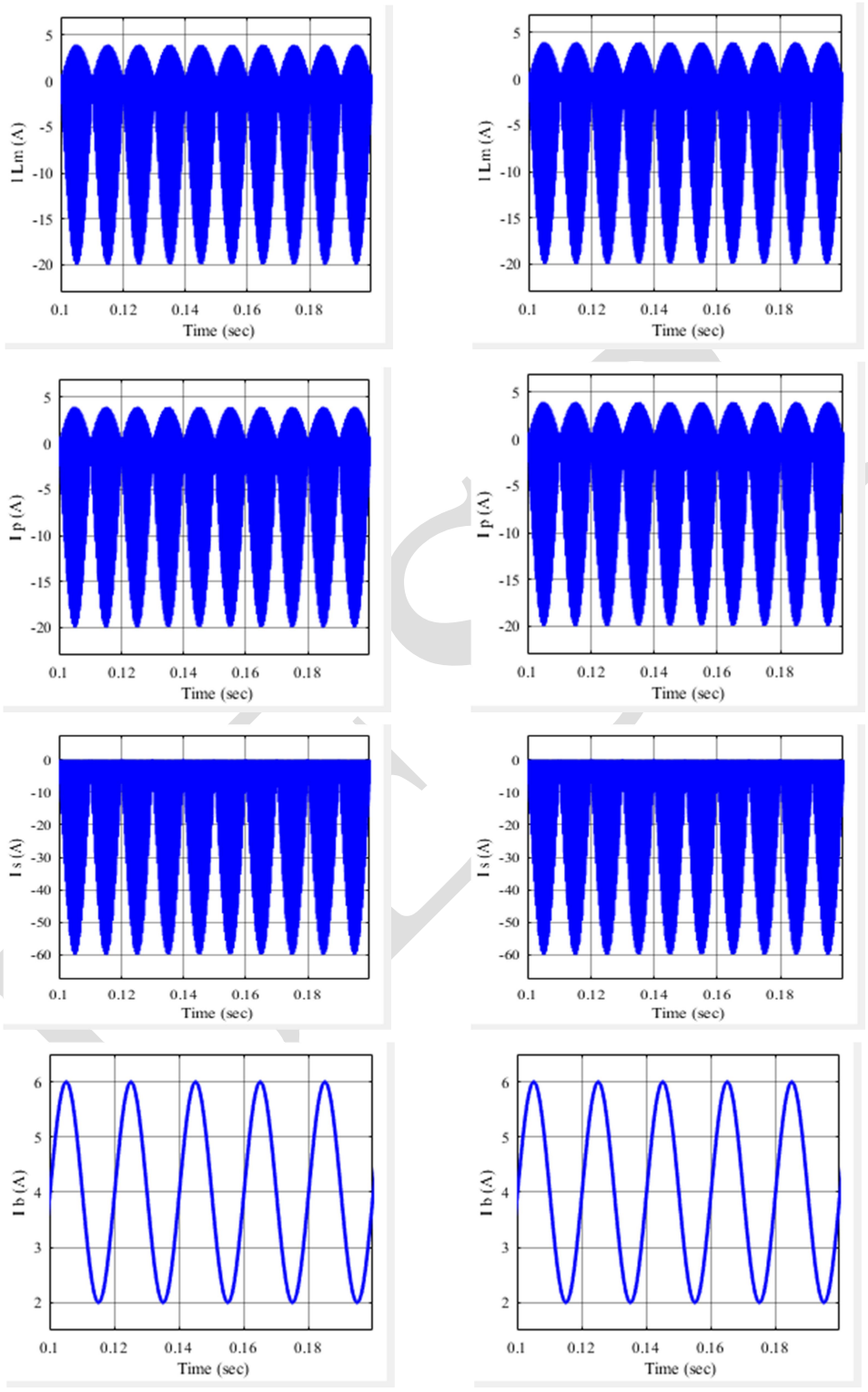

[A] [B]

Fig. 7 Shows the voltage and current strains over the charger components during G2V operation with a (a)72 V & (b)240 V battery-powered vehicle

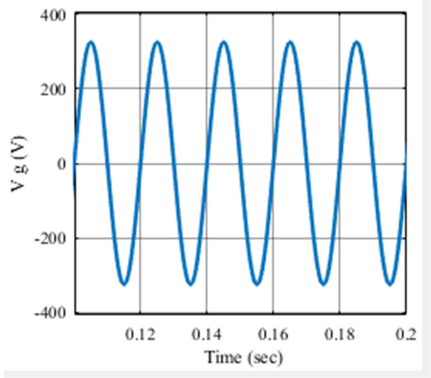
400
200
0
-200
-400
V g (V)
0.12
0.14
0.16
0.18
0.2
Time (sec)

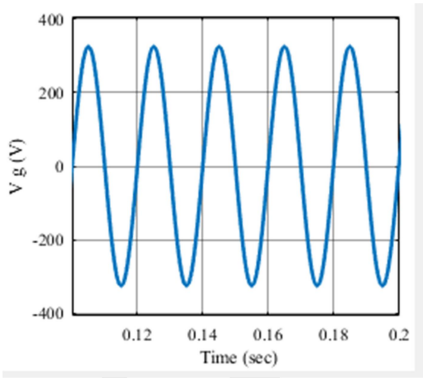
400
200
0
-200
-400
V g (V)
0.12
0.14
0.16
0.18
0.2
Time (sec)

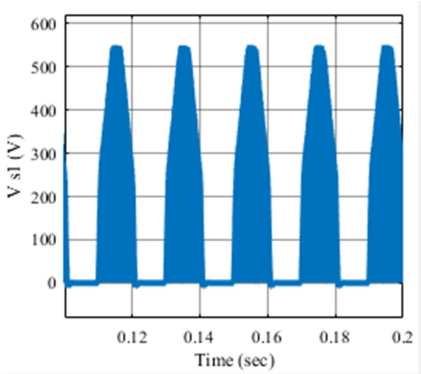
600
500
400
300
200
100
0
V s1 (V)
0.12
0.14
0.16
0.18
0.2
Time (sec)

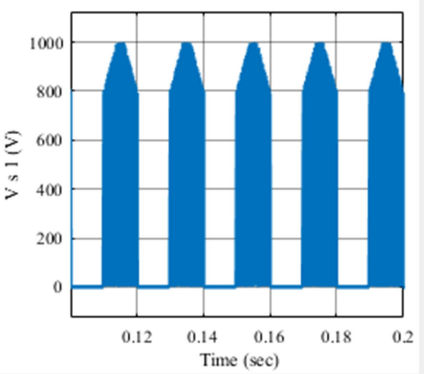
1000
800
600
400
200
0
V s 1 (V)
0.12
0.14
0.16
0.18
0.2
Time (sec)

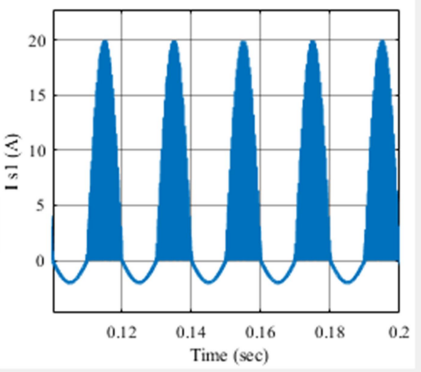
20
15
10
5
0
I s1 (A)
0.12
0.14
0.16
0.18
0.2
Time (sec)

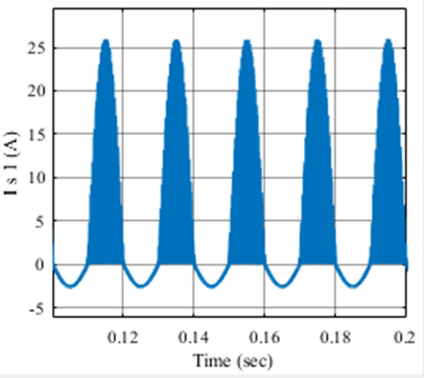
25
20
15
10
5
0
-5
I s 1 (A)
0.12
0.14
0.16
0.18
0.2
Time (sec)

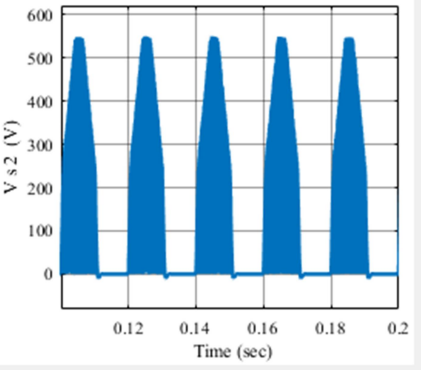
600
500
400
300
200
100
0
V s 2 (V)
0.12
0.14
0.16
0.18
0.2
Time (sec)

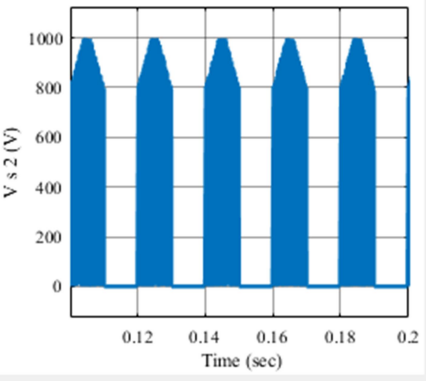
1000
800
600
400
200
0
V s 2 (V)
0.12
0.14
0.16
0.18
0.2
Time (sec)

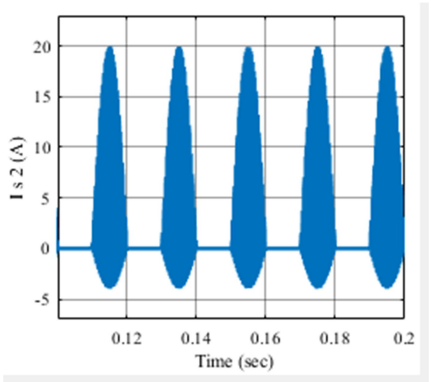
I s 2 (A)
Time (sec)

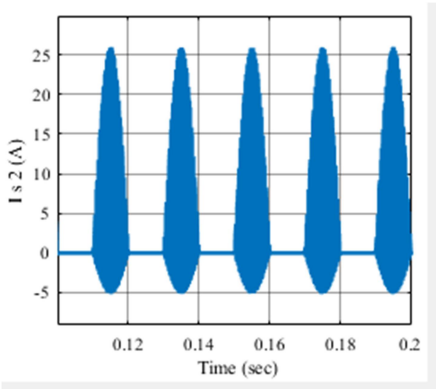
I s 2 (A)
Time (sec)

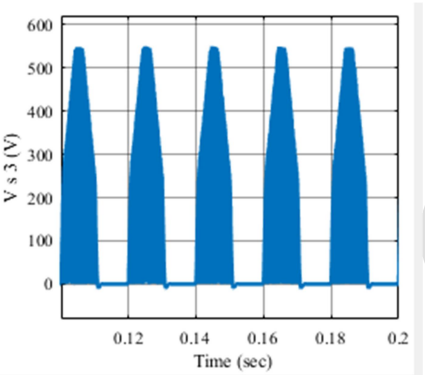
V s 3 (V)
Time (sec)

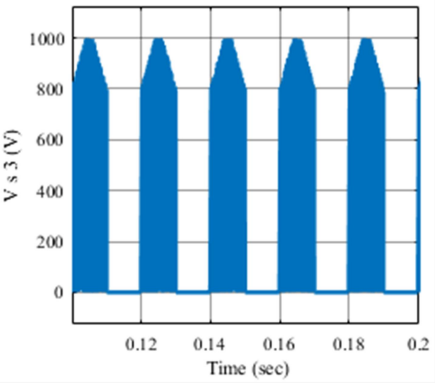
V s 3 (V)
Time (sec)

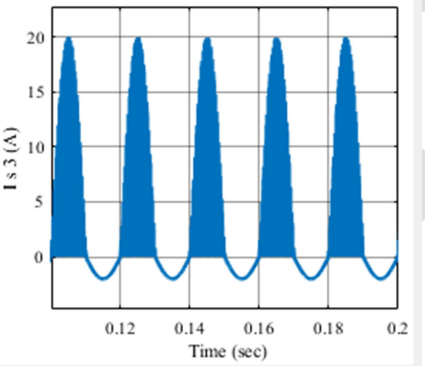
I s 3 (A)
Time (sec)

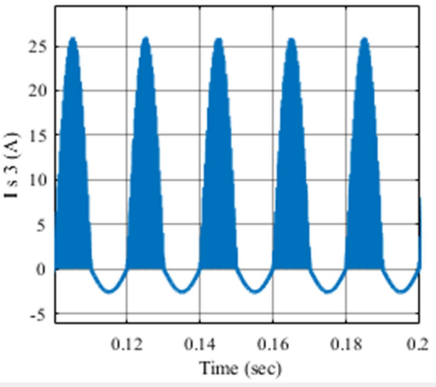
I s 3 (A)
Time (sec)

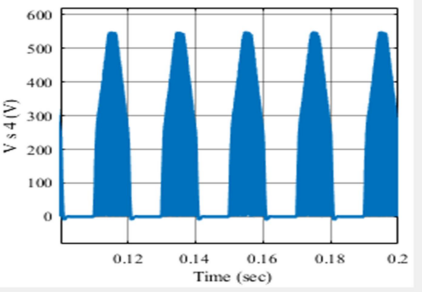
V s 4 (V)
Time (sec)

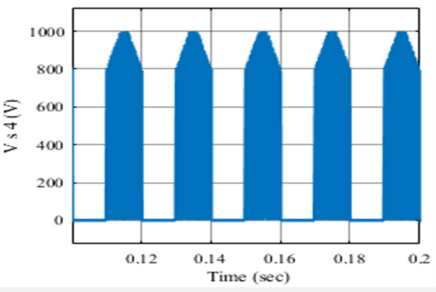
V s 4 (V)
Time (sec)

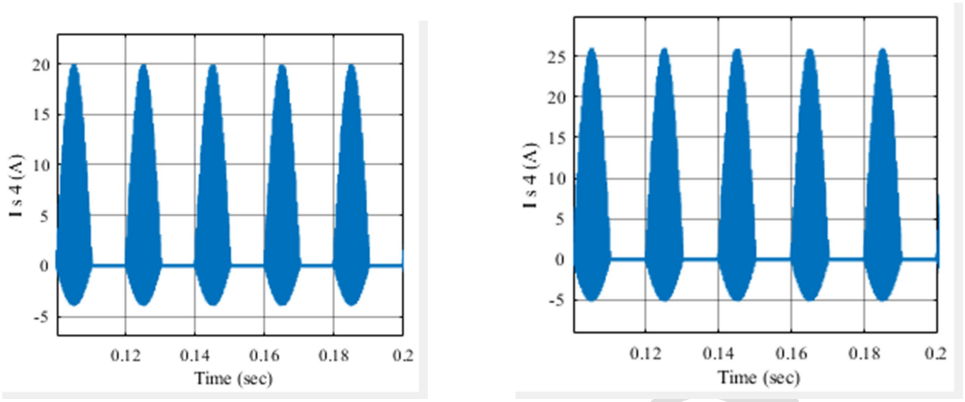

[A] **[B]**

Fig. 8 Shows the voltages currents across the switches of (a)72 V & (b)240V during G2V operation

C. Performance of Charger with Varying Grid Voltage

Variations in the amplitude of the grid voltage are addressed while analyzing the charger's efficacy in non-ideal conditions. Notably, a 20% drop in grid voltage is considered during voltage sag operation. As seen in Fig. 9(a), the grid voltage reduction is mirrored in the grid current escalation. As a result, the charging procedure remains constant current. Furthermore, the grid current meets the required power quality criterion, with a THD of 1.59%, as shown in fig. 9(a).

The charging operation of the provided charger with the grid voltage is carried out successfully, and the results are shown in Figure 9(b). Since the grid voltage surges, the grid current decreases, as shown in Fig. 9(b). This results in an undisturbed charging procedure, as demonstrated in Fig. 9(b). Furthermore, 2.65% grid current THD is obtained throughout the operation. As a result, the grid current complies with all applicable power quality criteria.

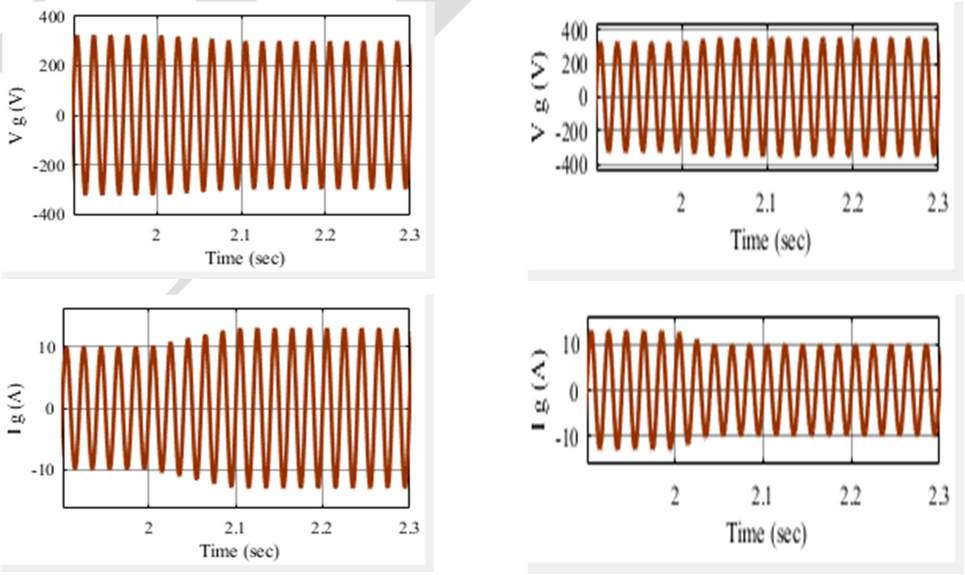

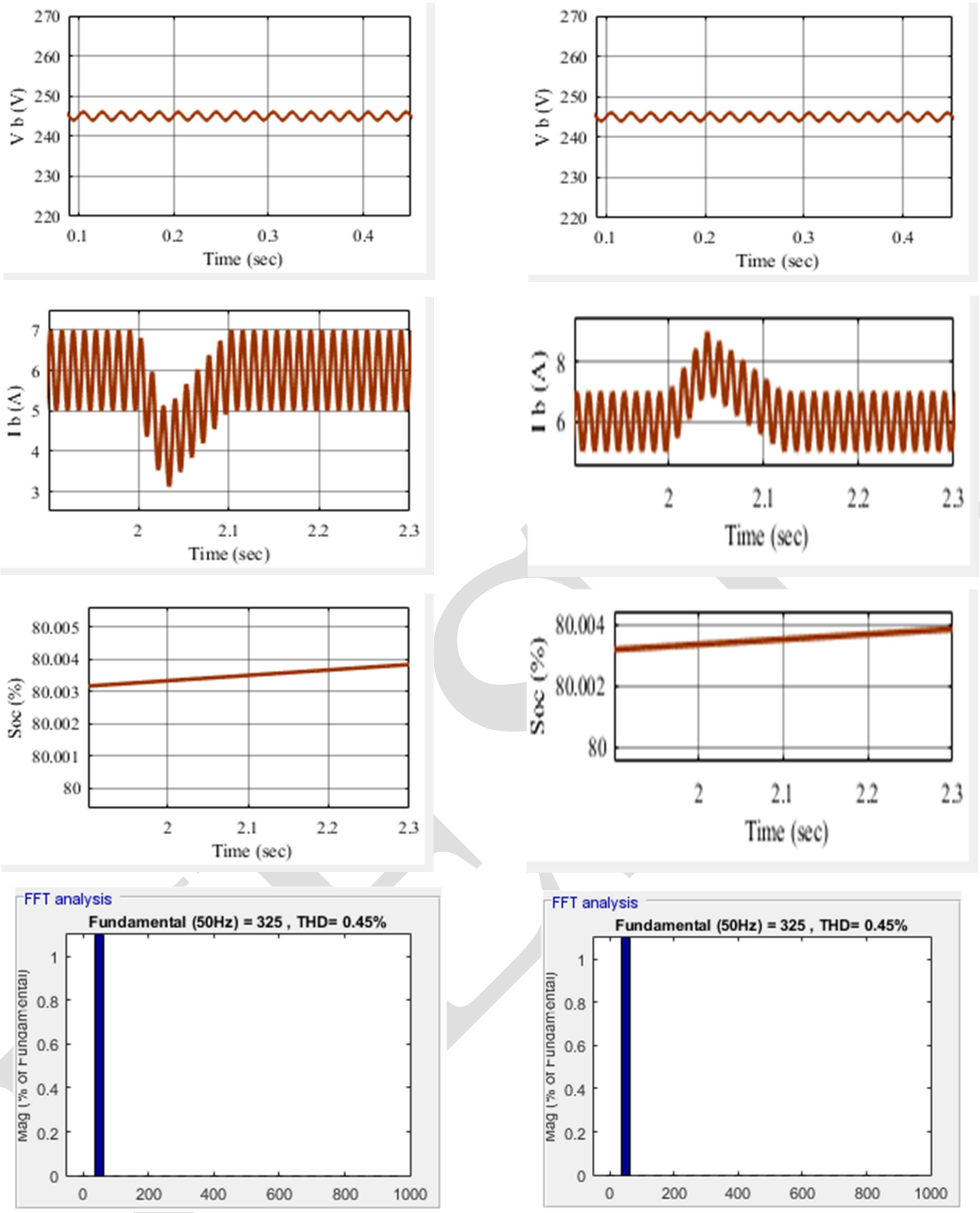

[A] **[B]**

Fig. 8 G2V operation during (a) sag, and (b) swell in the grid voltage.

D. Performance Analysis during V2H Operation

The V2H operation is used to evaluate the proposed charger's effectiveness during bidirectional operation, and the results are shown in Figs. 10(a)-(b). As shown in Fig. 10(a), the sinusoidal voltage is maintained at the point of intersection between the load and the charger. The non-linear load current is seen in Fig. 10(a). Out-of-phase load current and voltage measurements confirm that electricity is delivered to the load. The battery current is negative and regulated, as illustrated in Fig. 10a. As a result, the battery delivers electricity to the load. Figure 9(b) displays voltage and current across the charger's passive components during V2H operation. Figure 10(b) shows that the voltages and currents are regulated. As a result, the given charger performs well during V2H operation.

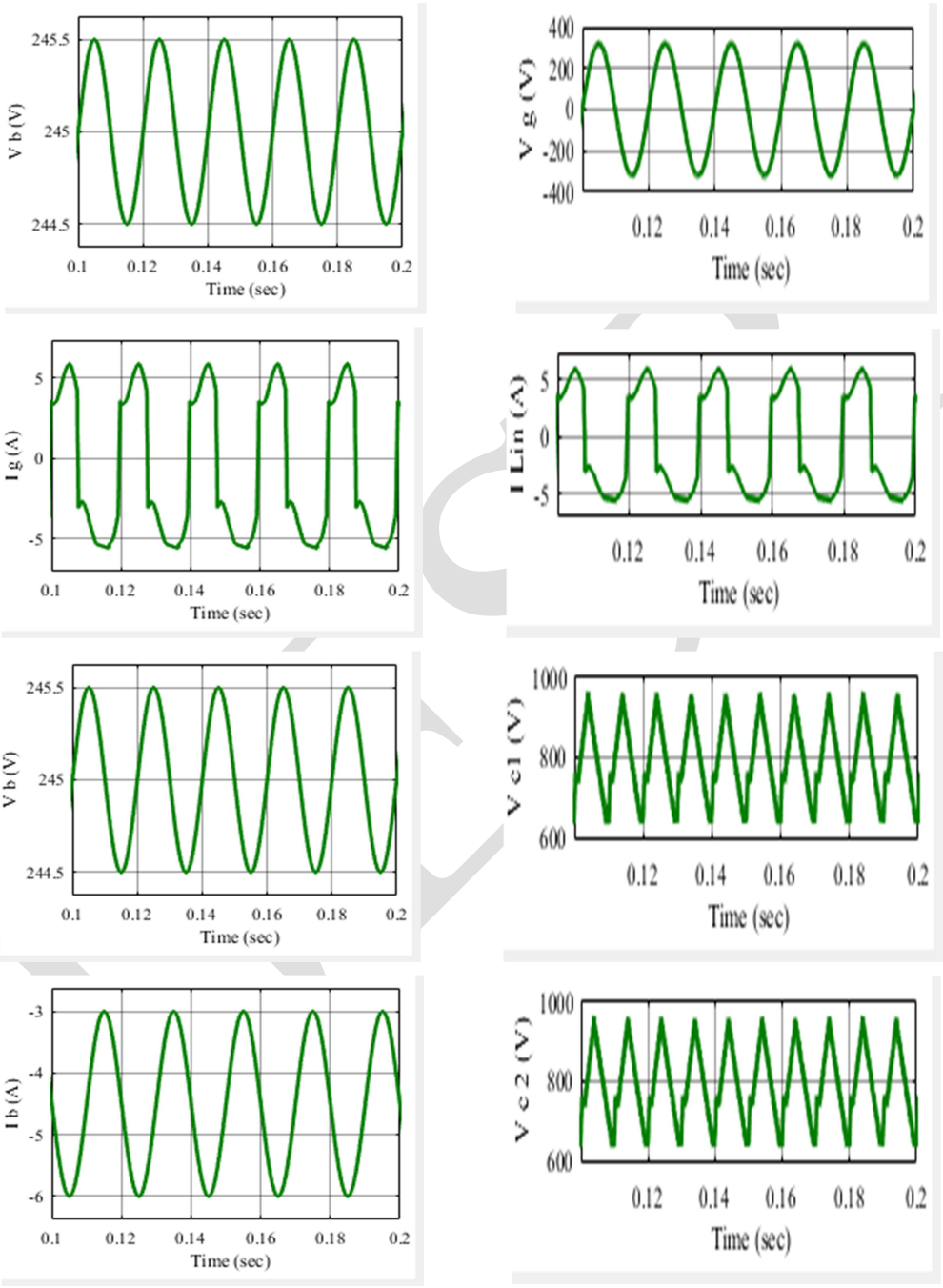
V b (V)
245.5
245
244.5
0.1 0.12 0.14 0.16 0.18 0.2
Time (sec)
V g (V)
400
200
0
-200
-400
0.12 0.14 0.16 0.18 0.2
Time (sec)
I g (A)
5
0
-5
0.1 0.12 0.14 0.16 0.18 0.2
Time (sec)
I Lin (A)
5
0
-5
0.12 0.14 0.16 0.18 0.2
Time (sec)
V b (V)
245.5
245
244.5
0.1 0.12 0.14 0.16 0.18 0.2
Time (sec)
V c1 (V)
1000
800
600
0.12 0.14 0.16 0.18 0.2
Time (sec)
I b (A)
-3
-4
-5
-6
0.1 0.12 0.14 0.16 0.18 0.2
Time (sec)
V c 2 (V)
1000
800
600
0.12 0.14 0.16 0.18 0.2
Time (sec)

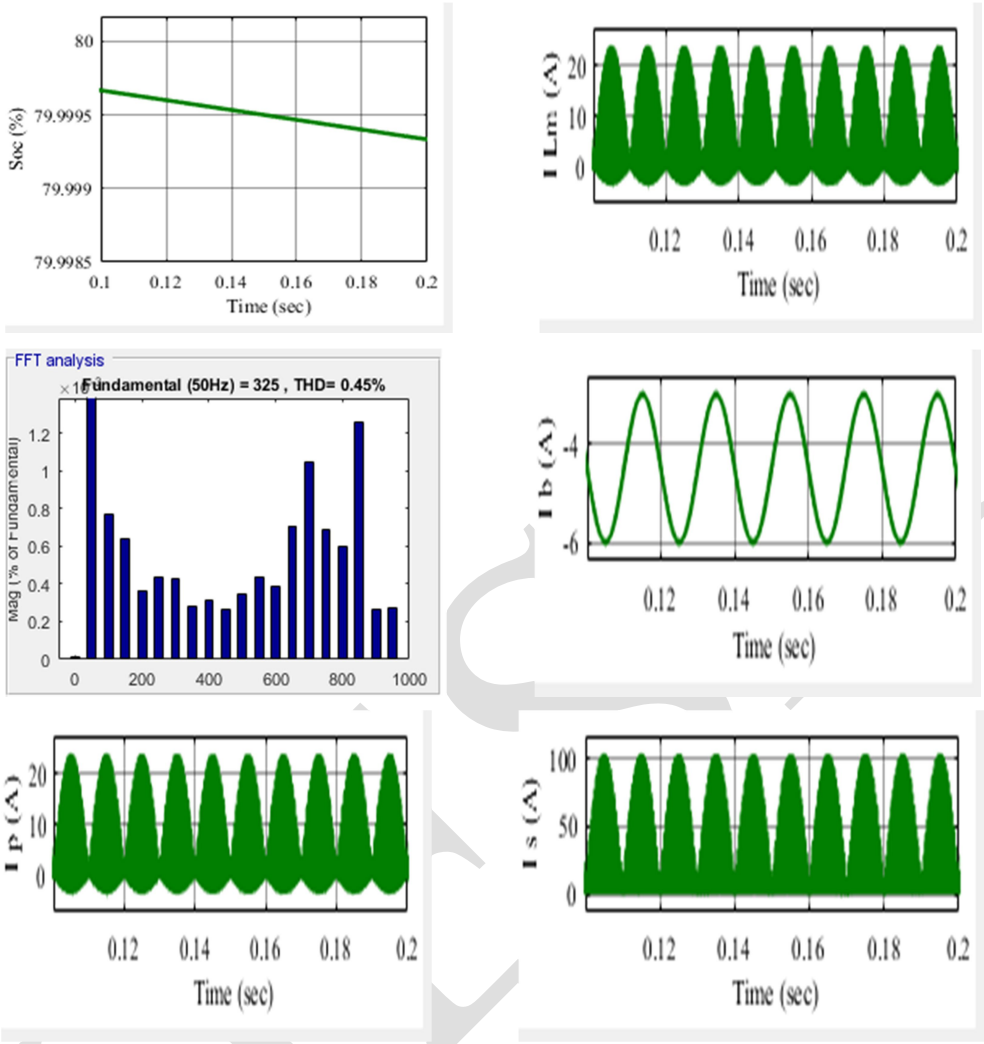

[A] **[B]**

Fig. 9 Results during the V2H operation

VII. CONCLUSION

An isolated single-stage bidirectional battery charger with a wide output voltage range is demonstrated. The given charger is built around a modified SEPIC converter-based bidirectional bridgeless converter. The fundamental DCM operation of the converter has been discussed. Furthermore, a control for regulating battery current during both G2V and V2H operation has been described. The provided charger's design and efficacy during G2V and V2H operation are evaluated and verified using simulation. To verify the wide output voltage functionality, a 72 V and a 240 V battery were charged. Furthermore, the controller's performance was tested under a variety of grid voltage circumstances. The charger met the necessary power quality standards during its grid-connected operation. Finally, an effective V2H operation has been proven. As a result, the provided charger's design and functioning were deemed to be satisfactory.

REFERENCES

[1] R. Kushwaha, B. Singh, and V. Khadkikar, "An Isolated Bridgeless Cuk-SEPIC Converter-Fed Electric Vehicle Charger," IEEE Trans. on Industrial Applications, vol. 58, no. 2, pp. 2512-2526, March-April 2022.

[2] H. Nazi, E. Babaei, S. Tohidi, and M. Liserre. "An Isolated SRC-Based Single Phase Single Stage Battery Charger for Electric Vehicles," IEEE Trans. Transp. Elect., Early Access, 2022.

[3] M. Abbasi, K. Kanathipan, and J. Lam, "An Interleaved Bridgeless Single-Stage AC/DC Converter with Stacked Switches Configurations and Soft-Switching Operation for High Voltage EV Battery Systems," IEEE Trans. on Industrial Applications, Early Access, 2022.

[4] M. Restrepo, J. Morris, M. Kazerani, and C. A. Cañizares. "Modeling and Testing of a Bidirectional Smart Charger for Distribution System EV Integration," IEEE Trans. on Smart Grid, vol. 9, no. 1, pp. 152-162, Jan. 2018.

[5] Fernandez, J. Sebastian, M. M. Hernando, P. Villegas, and J. Garcia, "Helpful hints for selecting a power-factor-correction solution for low- and medium-power single-phase power supplies," IEEE Trans. on Ind. Elect., vol. 52, no. 1, pp. 46-55, February 2005.

[6] M. Kwon and S. Choi, "An Electrolytic Capacitorless Bidirectional EV Charger for V2G and V2H Applications," IEEE Trans. on Power Elect., vol. 32, no. 9, pp. 6792–6799, September 2017.

[7] Jain, K. K. Gupta, S. K. Jain, and P. Bhatnagar, "A Bidirectional Five-Level Buck PFC Rectifier With Wide Output Range for EV Charging Application," IEEE Trans. Power Elect., 2022.

[8] Y. Yuan and Z. Zhang, "A Single-phase Vienna Rectifier with Wide Output Voltage Range," IEEE Trans. Transp. Elect. (Early Access).

[9] R. Kushwaha and B. Singh, "A Bridgeless Isolated Half Bridge Converter Based EV Charger with Power Factor Pre-regulation," IEEE Transp. Elect. Conf. (ITEC-India), pp. 1–6, 2019.

AUTHORS

Mr. P. Uday Kumar obtained his Bachelor of Technology in Electrical and Electronics Engineering from Sree vahini institute of science and technology in the year 2015.He completed M. tech in Sree vahini institute of science and technology in the year 2018. His areas of interests are Power Systems, Electrical Machines, Power Electronics and Devices, Electrical Circuits and Power system Analysis.

Mr. B .Sai Pavan Kumar obtained her Bachelor of Technology in Electrical and Electronics Engineering from sree vahini institue of science and technology, Tiruvuru, Andhra Pradesh, India. His areas of interests are Power Systems, Electrical Machines, and Power Electronics and Devices.

Mr. T. Venkata Krishna obtained his Bachelor of Technology in Electrical and Electronics Engineering from sree vahini institue of science and technology, Tiruvuru, Andhra Pradesh, India. His areas of interests are Power Systems, Electrical Machines, and Power Electronics and Devices.

Mr. SK. Karimulla obtained his Bachelor of Technology in Electrical and Electronics Engineering from sree vahini institue of science and technology, Tiruvuru, Andhra Pradesh, India. His areas of interests are Power Systems, Electrical Machines, and Power Electronics and Devices.